symmetry

MDPI

Article

A Symmetric Experimental Study of the Interaction Between Regular Waves and a Pontoon Breakwater with Novel Fin Attachments

Xiangcheng Lyu [1], Yifeng Yang [1,2,*], Chenhao Mi [1], Chi Man Tang [1], Lukman Adeboye [1], Mohamed Farhan [1], Stan Collins [1], Binjian Ou [1], Anson Wong [3], John Gordon Duffy [3] and Luofeng Huang [1,*]

[1] Faculty of Engineering and Applied Sciences, Cranfield University, Cranfield MK43 0AL, UK; xiangcheng.lyu.285@cranfield.ac.uk (X.L.); chenhao.mi.960@cranfield.ac.uk (C.M.); s.collins@cranfield.ac.uk (S.C.); binjian.ou.280@cranfield.ac.uk (B.O.)
[2] Department of Mechanical Engineering, University College London, London WC1E 7JE, UK
[3] DuPont, 1501 Larkin Center Drive, Midland, MI 48642, USA; anson.wong@dupont.com (A.W.)
* Correspondence: ucemanj@ucl.ac.uk (Y.Y.); luofeng.huang@cranfield.ac.uk (L.H.)

Abstract: Floating breakwaters are widely applied on the ocean water surface to protect human infrastructure from the destructive power of waves. This study designs and investigates the performance of a novel symmetric-pontoon floating breakwater with a symmetric pair of hydrofoils. Based at the Cranfield Ocean Systems Laboratory, the system was constructed and tested in various wave conditions using different fin configurations. The floating structure was anchored using a symmetric four-point mooring system. The tested waves were regular and symmetric perpendicular to the propagating direction. Key parameters, including the attenuated wave amplitude, motions of the breakwater, and the mooring forces, were measured. The wave parameters utilised for testing covered 1.61–5.42 relative wavelength to structural length, with wave heights of 3 cm and 5 cm. Results showed the 90° fin configuration can reduce wave transmission by up to 74%, with the lowest mooring forces at 3.05 relative wavelength, enhancing the performance of wave energy dissipation and structural seakeeping. At 90° setup, the mooring force was lowest at 2.41 relative wavelength. This research can inform novel designs of breakwaters to improve protection abilities for coastal cities and offshore infrastructures, especially renewable energy systems.

Keywords: floating breakwater; wave tank experiment; fin attachment; wave attenuation; mooring forces

Citation: Lyu, X.; Yang, Y.; Mi, C.; Tang, C.M.; Adeboye, L.; Farhan, M.; Collins, S.; Ou, B.; Wong, A.; Gordon Duffy, J.; et al. A Symmetric Experimental Study of the Interaction Between Regular Waves and a Pontoon Breakwater with Novel Fin Attachments. *Symmetry* **2024**, *16*, 1605. https://doi.org/10.3390/sym16121605

Academic Editor: Sergei Odintsov

Received: 2 October 2024
Revised: 18 November 2024
Accepted: 27 November 2024
Published: 2 December 2024

1. Introduction

The study of breakwaters was extensively conducted to document their designs, efficiencies, and impacts. Floating breakwaters (FBs) are more flexible and adaptable to changing water levels and wave conditions compared to bottom-fixed breakwaters. They are often less expensive to construct, requiring less material and labour for installation. FBs are easier to install and can be deployed as quickly as they can be relocated. Minimal adverse impacts on the surrounding marine environment have been noted during installation and operation, allowing ecological and sediment movement [1].

The hydrodynamic interaction between regular and irregular waves and FBs in shallow and intermediate waters was comprehensively investigated through experimental studies [2,3]. The research aimed to explore how incident wave characteristics and structural geometric properties influence the overall efficiency of FBs. By examining various configurations, the study revealed that the efficiency of floating breakwaters is strongly linked to the length-to-wavelength ratio and the draft-to-water-depth ratio. These relationships indicate that optimising these geometric parameters can significantly enhance wave energy dissipation. Moreover, a notable insight from the study was the comparative analysis between FBs and fixed breakwaters. It was found that, unlike a single fixed

breakwater, which primarily acts as a barrier, a FB with motions operates in a more dynamic manner. FB not only interacts with the incoming waves but also dissipates energy by absorbing a portion of it, thereby reducing wave transmission and enhancing wave attenuation [4]. The wave-attenuation performance of breakwaters is also influenced by the angle of inclination [5]. These findings underscore the importance of considering both wave characteristics and structural parameters when designing more efficient breakwater systems. Some breakwaters incorporate additional components, such as attached plates and nets. Research has demonstrated that equipping rectangular FBs with vertical plates as wave-dissipating elements significantly enhances their hydrodynamic performance, thereby improving structural efficiency while maintaining cost-effectiveness [6]. Comparative analysis indicates that the wave-attenuation performance of floating breakwaters fitted with wing plates differs substantially from that of conventional box-type breakwaters. By employing a parameterisation approach based on a multi-objective genetic algorithm (MOGA) to optimise the dimensions of wing plate floating breakwaters, findings confirmed that incorporating wing plates can markedly enhance the wave-attenuation performance of box-type floating breakwaters [7]. Consequently, attached plates are regarded as one of the most effective structural enhancements.

The length-to-wavelength ratio plays a significant role in determining an FB's effectiveness. The influence of FB layouts was examined by [8] in terms of wave transmission, loads along moorings and connectors, under oblique waves. Two layouts, characterised by different degrees of complexity (I- and J-shaped), and three obliquities (0°, 30°, 60°), were examined. With increased wave obliquity, the FB became more efficient due to the decrease in wave transmission and mooring forces. Under perpendicular wave conditions, increasing the complexity of the layout did not yield significant changes in wave transmission; however, there were notable variations in the forces acting on mooring systems and inter-module connectors. To evaluate wave blocking and energy absorption, a time-domain simulation of a pneumatic-type floating breakwater was conducted [9]. This research extended the fully nonlinear numerical wave tank (NWT) technique to include the analysis of restrained body motion using the mode-decomposition method within the acceleration potential field. The study revealed that incorporating a pneumatic damping system within the breakwater structure enhanced wave energy absorption by regulating the airflow velocity at the chamber's outlet. This mechanism allowed for more effective dissipation of wave energy. When compared to traditional box-shaped floating breakwaters, pontoons are equipped with a damping system demonstrated up to 20% higher efficiency. Additionally, an innovative design featuring wing structures and perforated sections was proposed, further contributing to enhanced performance [10]. The study emphasised the significance of Computational Fluid Dynamics (CFD) analysis in revealing wave slamming and water spraying as key factors in improving wave-attenuation performance. The transmission coefficient (K_t) was found to be 9% lesser than the traditional FB under the effect of wave slamming, and the K_t was about 5% reduced under the effect of water spraying. Ref. [11] analysed numerical simulations using CFD and reported that longer fins will yield lower K_t.

For a conventional breakwater, once it is constructed, it normally cannot adjust its geometry and shape based on different flow conditions. The rotation of the earth influences the complex wind patterns that drive the ocean wave, which keeps changing throughout the year. When the wave conditions change, it is key to note that the magnitude of the impact on the breakwater varies considerably. In such a case, the flexibility to alter the breakwater parameters can be quite efficient, bringing about the desirable structural changes in the face of variable wave conditions. Here, the concept of bio-inspired fins as an attachment can be crucial in improving the effectiveness of FB. In shipping terms, it is referred as bilge keel. The concept draws inspiration from fish. It is widely used in reducing the roll motion of ships by generating vortices when the ship rolls, dissipating the kinetic energy and improving damping of the ship [12]. Vortex generation lowers the transmission coefficient by dissipating wave energy, disrupting wave coherence, and redirecting energy around

structures, helping to block or weaken transmitted waves [13]. The same principle can be extended to FBs to reduce the Kt. Moreover, a fin attachment with configurable angles can be used to vary the length and draught of the FB, depending on which angle the fin is positioned.

The effectiveness of a box-type floating breakwater decreases as the wavelength relative to the breakwater's length increases. Typically, these structures are most effective against short-period waves; however, for long-period waves, particularly those with wavelengths significantly exceeding the length of the breakwater, wave energy transmission increases, resulting in reduced effectiveness. Studies have shown that pontoon types with air damping are more effective than conventional box-type breakwaters in certain conditions [9]. However, research has yet to comprehensively explore the impact of configurable fin attachments on pontoon-type breakwaters, an area that remains under-investigated despite related studies addressing similar modifications and their influence on wave-breaking efficiency under varying wave conditions. Adjusting the angle of these attachments could potentially enhance wave energy dissipation, adapting to changing wave conditions more effectively [14]. In this context, this project is motivated to investigate the influence of variable fin angle adjustment on the wave-induced motion and mooring forces behaviour. Consequently, combining a pontoon structure with a configurable fin attachment system emerges as a valuable area of interest for current and future research. Considering all the factors affecting the efficiency of floating breakwaters in reducing transmission coefficients, and drawing inspiration from past design iterations, this project involves the design, construction, and testing of a pontoon-shaped breakwater with a fin attachment adjustable to various angles at Cranfield University's wave tank facility.

This paper is organised as follows. The prototype design is presented in Section 2, including Section 2.1 for the geometry and materials, and Section 2.2 for the down scaling for experiments. The experimental cases and conditions are developed in Section 3, including Section 3.1 for wave tank, Section 3.2 for experimental cases, and Section 3.3 for sensors. The experimental results are presented and discussed in Section 4. Section 5 summarises this research and provides recommendations for future work.

2. A Novel FB with Fin Attachments

This study designed and investigated the performance of a novel symmetric-pontoon floating breakwater with a symmetric pair of hydrofoils. Based at the Cranfield Ocean Systems Laboratory, the system was constructed and tested in various wave conditions using different fin configurations. The floating structure was anchored using a symmetric four-point mooring system. The tested waves were regular and symmetric perpendicular to the propagating direction.

2.1. The Geometry of the Prototype

Both pontoon-type and box-type breakwaters feature relatively simple structures, making them easy to manufacture, as shown in Figure 1. However, for the same dimensions, the pontoon-type requires less material, which can reduce production costs. Both floating breakwater types employ wave attenuation by reflecting incident waves off their surfaces. However, the pontoon breakwater's gap between floaters allows for turbulent dissipation [15], increasing wave energy dissipation. Hence, the pontoon breakwater was selected as the primary structure, as shown in Figures 1b and 2a. The performance of a breakwater is dictated by its own dimension [16]. The design of dimensions is introduced in Tables 1 and 2, and the scaling is introduced in Section 2.2. In this application, inertial forces are more significant than viscous forces. To maintain kinematic and dynamic similarity, the impact of viscosity is usually disregarded, with the Froude number and Strouhal number employed as substitutes for the Reynolds number, as shown in Table 3.

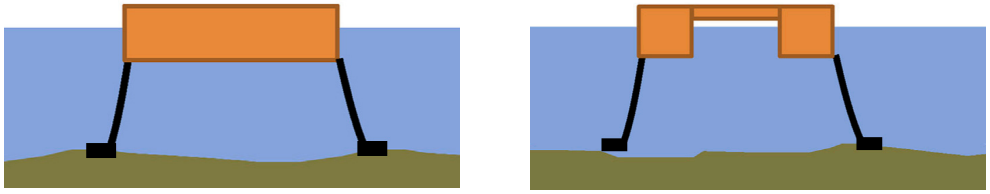

(**a**) (**b**)

Figure 1. Illustration of floating breakwater (**a**) box type (**b**) pontoon type.

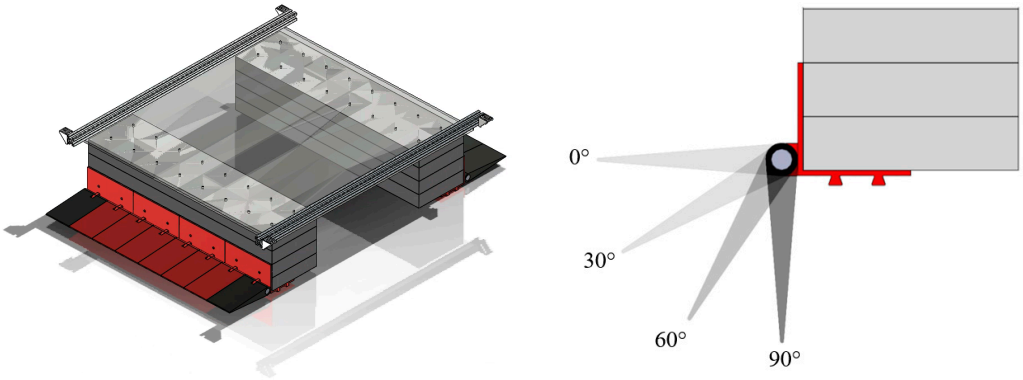

(**a**) (**b**)

Figure 2. 3D models of breakwater (**a**) pontoon-type with fin attachment (**b**) fin attachment installed at different angle settings.

Table 1. Floating structure dimensions for model scale and full scale.

Dimension	Symbol	Model-Scale	Full Scale
Length	L_m	800 mm	8000 mm
Height	h_m	200 mm	2000 mm
Width	B_m	860 mm	8600 mm
Width per raft	b_m	200 mm	2000 mm
Draught	d_m	100 mm	1000 mm
Length of fin	l_m	170 mm	1700 mm

Table 2. Configurations of the mooring system.

Mooring System Type	Taut Leg
Length of each mooring line	2500 mm
Angle of each mooring line	41.0°

To bolster the wave-dissipation capacity of the floating breakwater, a novel fin attachment was developed, as shown in Figure 2, inspired by the observed principles in fish, which utilise their gills and pectoral fins to execute abrupt stops during swimming. Furthermore, this attachment serves to augment both the draught and the reflective surface area. Moreover, it can induce vortices in the water, provoking energy dissipation through the turbulence [17]. When the fin attachment is installed at different angles, its primary wave dissipation mechanisms vary. At 0°, the main mechanism involves vortex generation, while at 90°, it primarily reflects waves. Therefore, this study primarily discussed the performance of different fins at various angles. The shape of the fin consists of two sloping surfaces that are tangential to a cylinder.

The mooring system (as shown in Figure 3 and Table 2) consists of four taut polyester ropes of 0.5 mm^2 cross-sectional area connected at the four edges of the structure [18–20]. The attachment points of the mooring system on the floating structure were positioned

slightly above the splash zone and water level, which helps protect the force sensors from short-circuit damage from water ingress. The other reason is that the alternative connection point would have been on the vertical wall of the main body of the breakwater, which is composed of extruded polystyrene (XPS) foam. XPS is known for its lightweight closed cell foam design that offer high mechanical strength and buoyancy performance, and hence, it is used in building insulation and buoyancy applications where compressive strength and moisture resistance are important. It also exhibits stable chemical properties, corrosion resistance, dimensional stability, and ease of processing [21]. Despite these characteristics, XPS is not designed to support the cyclic nature of the mooring force imposed upon it by the wave loading in the long term. Hence, the attachment points for the mooring system were designed accordingly.

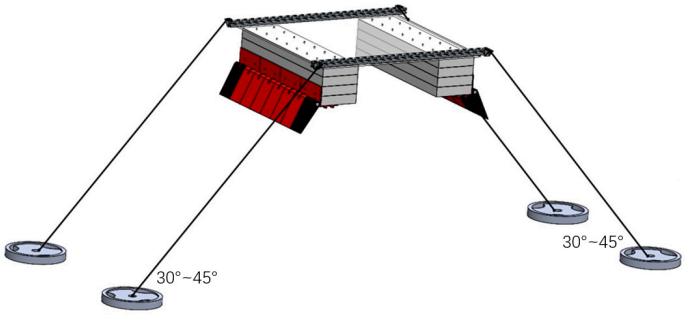

Figure 3. 3D illustration of the breakwater model with mooring attached.

The density of Styrofoam is 38.44 kg/m^3 [21]. The upper part of the breakwater was then connected with a Perspex Acrylic cast sheet. Its transparency also facilitates convenient inspection of breakwater internal structures. In the experimental setup, the fin was manufactured using Polylactic Acid (PLA). It is noted for its excellent printability, making it a prime candidate for 3D printing. This material also boasts excellent elasticity, outstanding thermal stability, minimal shrinkage, and biodegradability. Stiffening members are required to consolidate the acrylic and Styrofoam assembly. Aluminium profiles were selected based on their many excellent mechanical and physical properties [22]. Figure 4 shows the constructed prototype and its deployment in a wave tank facility.

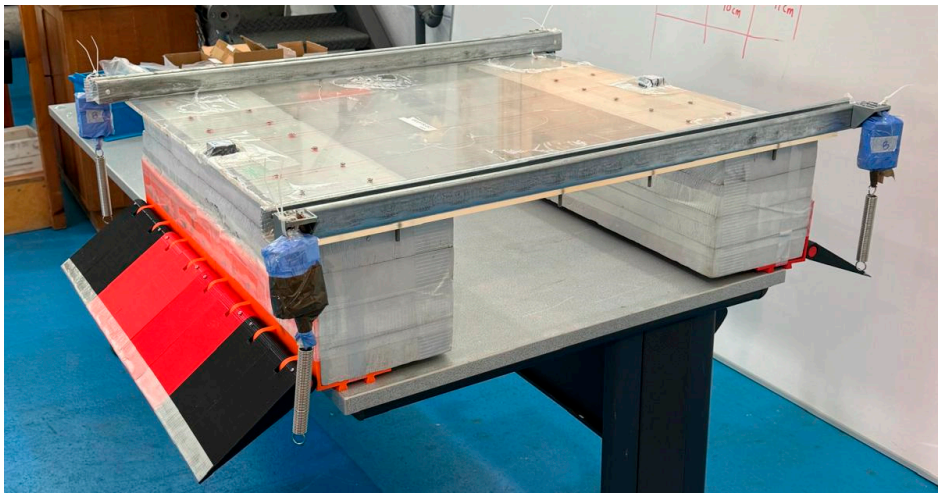

(**a**)

Figure 4. *Cont.*

(**b**)

Figure 4. (**a**) Experimental model of breakwaters. (**b**) Experimental model of breakwaters in a wave tank.

2.2. Scaling of the Experiment

Each module comprised two rectangular floaters and two rows of fin attachments. In the study, a significant wave height of 1 m was considered, while scaled down by a factor of 10, as introduced in Table 1. Froude scaling was then used to determine the structural length and height. Based on the principles of Stokes wave theory, the wavelength of the designed waves ranged approximately from 12 to 43 metres in the real world. A larger ratio of wavelength (λ) to structure length (L = 8 m) corresponded to relatively longer waves to the breakwater, generally corresponding so that more waves can pass through the breakwater. Typically, the width-to-wavelength ratio falls within the range of (λ / L = 1.5–5.04) [14]. Furthermore, considering the impact of fin-like attachments on both width and draught, the breakwater width was set at 8.6 m in full scale and 0.86 m in model scale. Therefore, the combined width of the full-scale breakwater with fin attachments on both side was 11.40 m.

To minimise any interference from the outer wall of the water tank in the experiment, the model-scale structure width was selected at 0.86 m, much smaller than the tank width of 1.5 m.

Over 90% of the total wave energy was concentrated within three times the wave height beneath the free surface [14]. Deepening the draught can enhance wave attenuation, and it is imperative for the breakwater height to surpass the wave height [14]. Additionally, fin attachment will deepen the draught. To ensure an ample reserve of buoyancy, the breakwater height was set at 2 m. Half of this height remained above the water surface, referred to as freeboard, while the rest is draught and was 1 m. Additionally, the length of the fin attachments was 1.7 m in full scale and 0.17 m in model scale. The fins were installed on both sides of the structure, and the width of the breakwater increased by twice the length of the fins from 0.8 m to 1.14 m.

Throughout the scaling-down process, it was imperative to maintain the constancy of the Froude number [23]. The scaling ratio is shown in Table 3.

Table 3. Froude scaling summary for model and prototype.

Quantity	Prototype-Model Ratio	Scale Relationship	Scale Factor
Linear dimensions	L_P/L_m	S	10
Linear Velocity	V_P/V_m	$S^{1/2}$	$10^{1/2} = 3.162$
Acceleration	a_P/a_m	1	1
Area	A_P/A_m	S^2	$10^2 = 100$
Volume	∇_P/∇_m	S^3	$10^3 = 1000$
Angle	α_P/α_m	1	1
Angular Velocity	$\dot{\alpha}_P/\dot{\alpha}_m$	$S^{-1/2}$	$10^{-1/2} = 0.316$
Wave Height	H_P/H_m	S	10
Wavelength	λ_p/λ_m	S	10
Wave Period	T_P/T_m	$S^{1/2}$	$10^{1/2} = 3.162$
Wave Frequency	f_P/f_m	$S^{-1/2}$	$10^{-1/2} = 0.316$
Water density	ρ_P/ρ_m	γ	1.025
Mass	m_P/m_m	γS^3	$1.025 \times 10^3 = 1025$
Force	F_P/F_m	γS^3	$1.025 \times 10^3 = 1025$
Moment	M_P/M_m	γS^4	$1.025 \times 10^4 = 10{,}250$
Power	P_P/P_m	$\gamma S^{7/2}$	$1.025 \times 10^{7/2} = 3241.33$

3. Experimental Facility and Setups

3.1. Wave Tank

The experimental tests of this project were carried out in a wave tank located at Cranfield University. The wave tank comprised three essential parts, as introduced in Figure 5, including a water tank, a wave maker, and an artificial beach. The water tank is a simple glass-made tank for containing water. The glass allows users to observe wave behaviours. This wave tank has the capability to generate wave heights ranging from 0.005 m to 0.28 m, with wave frequencies from 0.1 Hz to 1.1 Hz. In the present experiment, the still water depth was set to be $d = 1.5$ m, the length of the wave tank was $l_t = 30$ m, and the height of the wave tank was $l_w = 1.5$ m. The absorption region featured an artificial beach made from a curved steel plate, simulating a beach's slope and curvature. The generated waves are absorbed in the region. With a wave-absorption efficiency of around 97% [24], only a fraction of the incident waves are reflected by the beach. The reflected waves by the beach would have no influence on the experimental setup as there is sufficient distance between the absorption zone and the working zone. This distance would cause dissipation of the reflected waves.

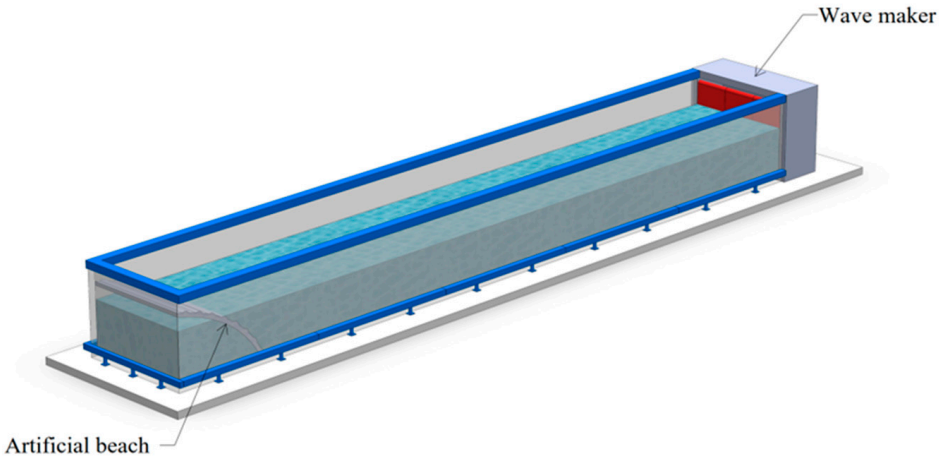

Figure 5. 3D illustration of the wave tank.

3.2. Experimental Cases

To comprehensively study the performance of the floating breakwater under different regular wave conditions, a range of experimental cases were designed. There were different model settings and wave parameters that needed to be varied in the experiments (as shown in Table 4).

- Without fin attachment: First, the breakwater model without any fin attachment should be tested. The result could be useful for assessing the significance of the fin attachment and comparing the performance of the breakwater with and without the fin.
- With fin attachment—installation angle relative to horizontal plane: From the design of the fin attachment, it could be adjusted to four installation angles, which are 0°, 30°, 60°, and 90°, relative to the horizontal plane.

Table 4. Wave parameters of experimental and real-world scenarios.

No.	Experimental Values			Real-World Values		
	H[m]	λ[m]	f[Hz]	H[m]	λ[m]	f[Hz]
1	0.06	4.337	0.6	0.6	43.37	0.190
2	0.06	3.186	0.7	0.6	31.86	0.221
3	0.06	2.440	0.8	0.6	24.40	0.253
4	0.06	1.928	0.9	0.6	19.28	0.284
5	0.06	1.561	1.0	0.6	15.61	0.316
6	0.06	1.290	1.1	0.6	12.90	0.348
7	0.1	4.337	0.6	1	43.37	0.190
8	0.1	3.186	0.7	1	31.86	0.221
9	0.1	2.440	0.8	1	24.40	0.253
10	0.1	1.928	0.9	1	19.28	0.284
11	0.1	1.561	1.0	1	15.61	0.316
12	0.1	1.290	1.1	1	12.90	0.348

For the wave height, in the tests, only 0.06 m and 0.1 m were chosen because they were the moderate values for the model. Smaller wave heights would result in mild wave conditions, which the results and data obtained would be insignificant, while larger wave height would make the condition too vigorous [25].

For the wave frequency, the wave maker could produce waves from 0.5 Hz to 1.1 Hz. Since 0.5 Hz was considered to be too calm for the model, the frequency range for the tests varied from 0.6 Hz to 1.1 Hz, with a 0.1 Hz increment for each successive test.

The dispersion equation was used to describe the propagation behaviour of water waves under different water-depth conditions and to explain the relationship between wavenumber, wavelength, wave speed, and frequency. During the experiment, different wave frequencies were set for the wave tank to adjust the incident wave parameters. The wavelength was then calculated using the following Equations (1)–(3):

$$k = 2\pi/\lambda \tag{1}$$

$$k\tanh(kd) = \frac{\omega^2}{g} \tag{2}$$

$$\omega = 2\pi f \tag{3}$$

where k is wave number, d is water depth, ω is angular frequency, and g is gravitational acceleration.

A suitable interval in-between each test was adopted to ensure that the water surface was calm from the previous wave interactions, thus avoiding data contamination by re-reflected waves from the wavemaker [26]. The FB was placed in the appropriate region in the wave tank, the working zone. A repeat of the selected experimental cases was done, and the data was checked for repeatability.

3.3. Sensors

In the experiments, a total of five sensors were used, which could be classified into three types. These sensors include force sensors, inclinometers, and wave gauges. By deploying these sensors, the experiments aimed to gather comprehensive data that was crucial for evaluating the developed floating breakwater performance, effectiveness, and durability. The installation positions of the sensors and the model setup are shown in Figure 6. The floating breakwater was subjected to motions in the six degrees of freedom (DoFs) in the wave tank due to the oscillating nature of the waves. Three of the motions can be described as translational displacement in the x, y, and z directions. These motions are referred to as surge, sway, and heave, respectively. The corresponding rotational motions about the same axes are known as roll, pitch, and yaw, respectively. In the study, three motion data sets are of interest, namely heave, surge, and pitch, as indicated in Figure 7 below.

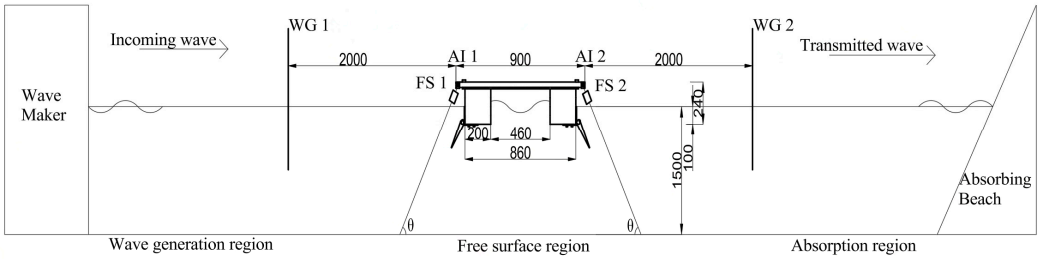

Figure 6. Illustration of the experimental setup.

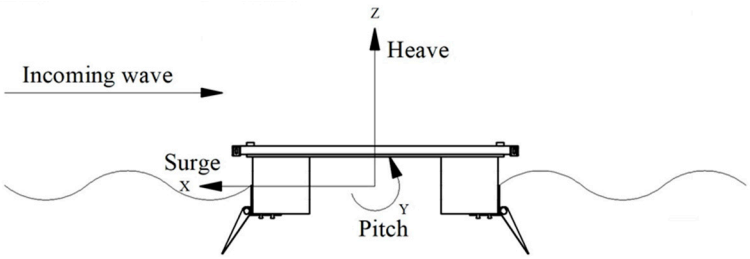

Figure 7. Motion schematics of the floating breakwater.

3.3.1. Force Sensors

This sensor should be placed in-between the breakwater structure and the mooring line, so that it can act as an extension of the mooring line while measuring the force acting on the line. To achieve this, the sensor was first tied with the hooking hole using cable ties, which were originally for the mooring system. Then, a spring was installed on the hook that was outstretched from the sensor itself, to provide damping and suspension for the structure. At last, the mooring line was attached to the spring. The force sensor data in time domain was processed for it to be useful. The load series was established, and a Fourier transformation analysis was performed in a similar fashion as those of the wave gauges and the motions. The force sensor model is the Go Direct Force and Acceleration Sensor, with a measurement accuracy of 0.1 N, a range of $\pm$50N, and a resolution of 50 Hz. The spring coefficient was measured to be 454.4 N/m.

3.3.2. Accelerator-Inclinometers

An accelerator-inclinometer is a device used to measure the translational and rotational motion in the three orthogonal planes. The device can collect and record motion data in six degrees of freedom. For simplification of the analysis, the relevant measurement of interest shall be the pitch angle, heave, and surge motions. Two accelerator-inclinometers were used in the experiment, one installed in the front and another one in the rear. It was needed to make sure that the sensors were installed aligning on the centreline of the

breakwater to ensure accurate results. The device was installed with its x-axis oriented along the length of the wave tank. The accelerator-inclinometer model is WT901C, with an accuracy of 0.05° for static measurements and 0.1° for dynamic measurements. It has an angle range of ±180° for the X and Z axes and ±90° for the Y axis. The sensor operates at a resolution of 50 Hz.

3.3.3. Wave Gauges

By installing wave gauges both on the upstream area and the downstream area in the wave tank along the centre line of the tank, the water surface elevations before and after passing the breakwater could be measured. The wave gauges were calibrated before use, to ensure accurate, consistent, and repeatable values are obtained when used.

4. Results and Discussion

This section provides a concise and precise description of the experimental results, along with their interpretation and the experimental conclusions drawn. The analysis methods referenced here are based on in the cited studies. To minimise the influence of random experimental errors, each test was repeated at least three times. The coefficient of variation was calculated for each set of measurements. The uncertainty level was identified to be less than 3%.

Meanwhile, the accelerations along the three axes were recorded by the accelerometer, which calls for further treatment of the data. The data processing involved analysis of the motion history, where a Fast Fourier Transformation (FFT) used double integration of the acceleration data to obtain their corresponding displacements. The experiment primarily analysed motion in three degrees of freedom: surge, heave, and pitch. These motions represent the oscillation amplitudes relative to the mean position of the floating breakwater under the influence of waves. To nondimensionalise the resulting values of the motions, the term response amplitude operator (RAO) is introduced, expressed as the ratio of the amplitude of the motions of the floating breakwater to the amplitude of the incoming wave. The RAOs for the surge, heave, and pitch motions are defined as given below in Equations (4)–(6) [27]:

$$\mathrm{RAO}_{\mathrm{surge}} = \frac{A_{surge}}{A\cosh(kd)} \tag{4}$$

$$\mathrm{RAO}_{\mathrm{heave}} = \frac{A_{heave}}{A} \tag{5}$$

$$\mathrm{RAO}_{\mathrm{pitch}} = \frac{\Theta_{pitch}}{kA} \tag{6}$$

where d denotes the still water depth as defined in Section 3.1, and A_{surge}, A_{heave}, and Θ_{pitch} denote the motion amplitudes for surge, heave, and pitch motion, respectively.

4.1. The Transmission Coefficient of the Model

To evaluate the performance of the breakwater, the transmission coefficient was used. The incident wave amplitude A_i was measured by WG1 when the structure was not deployed in the tank. During the experiment, the transmitted wave height A_t was measured using WG2. In such a case, the transmission coefficient was evaluated from Equation (7):

$$K_t = \frac{A_t}{A_i} \tag{7}$$

It was seen that the finned configuration with 90° orientation had the lowest Kt for both the 3 cm and 5 cm incident wave amplitudes, as seen in Figures 8 and 9 below. Between 41% and 74% wave attenuation was realised by the fin attachment at 90° compared to the setup with no fin attachment. The best outcomes of Kt for the breakwater with 90° fin attachment occurred between λ/L of 1.5 and 2.5. Outside of this range, its performance was not remarkable. Also, it was noted that as the angle of inclination decreased from

90° to 0°, the wave-damping effectiveness of the structure declined, implying an inverse relationship between the fin attachment and Kt. The same observations in Figure 8a,b present Kt variation with frequency at 3 cm and 5 cm incident wave amplitudes.

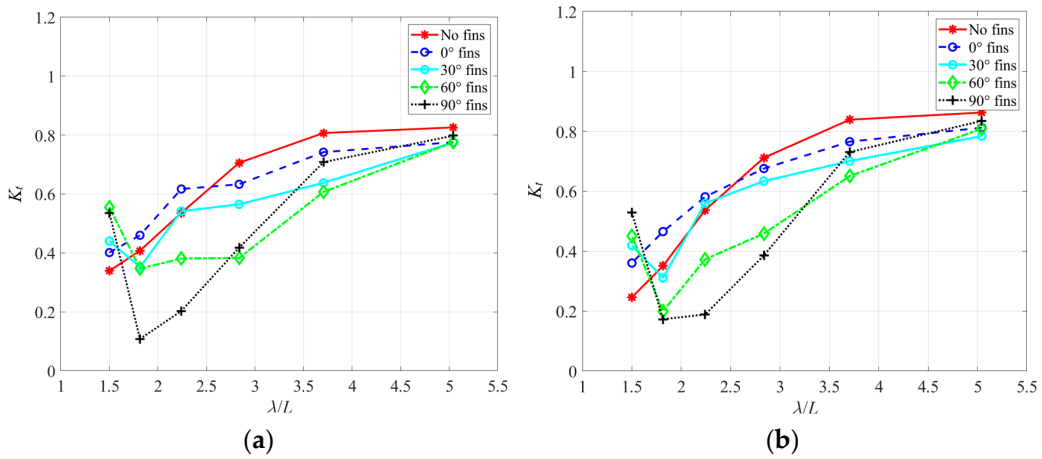

Figure 8. Transmission coefficient variation with λ/L at (**a**) 3 cm and (**b**) 5 cm incident wave amplitude.

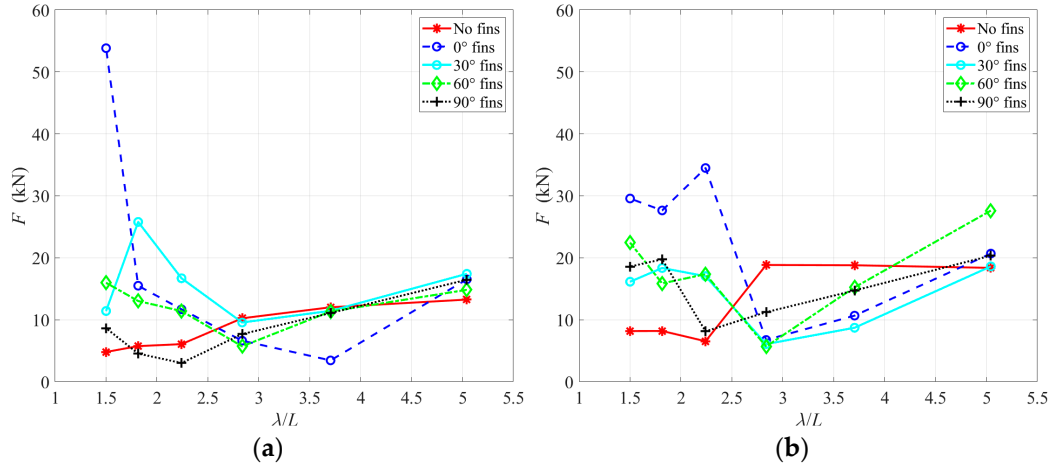

Figure 9. Mooring line forces (N) variation with λ/L for (**a**) 3 cm and (**b**) 5 cm incident wave amplitudes.

The 90° finned configuration was able to achieve a wave-reduction effectiveness of over 80% because, at 90°, the draught of the structure had increased from its initial 10 cm to 25 cm by combining the effective length of the fin (15 cm). The component of the incident waves below the water surface was effectively attenuated by the increased draught. This was particularly true as stated by [28], that 95% of the wave energy was located between the water surface and a quarter of the wavelength below it. It follows that a greater draft depth at 90° would dampen the wave energy even more as wave energy decreases exponentially from the surface downward. Also, increasing the draught of any floating breakwater often compensates for its width requirement, thus reducing the engineering cost in the context of material cost, construction difficulty, and safety requirements [14].

4.2. Load on the Mooring System

To keep the breakwater in the middle position of the wave tank, and prevent it from drifting with the waves, the mooring lines were pre-tensioned with force in the range of 14 N to 22 N. The pre-tensioning was applied prior to starting the wave machine and maintained during each run of the experimental case. Pre-tensioning was applied before each experiment to ensure that the spring does not loosen during testing [29]. The data in the figure represented the results after removing the pre-tensioned force.

The mooring forces obtained via the approach described above, when graphed, produced the illustrations in Figure 9a,b. Considering the plot of mooring forces variation with frequency for the lower incident wave amplitude of 3 cm illustrated in Figure 9a, the forces exerted on the floating structure's mooring lines when the fin attachment angle was set at 90° appear to be lower than the mooring forces in the setup with no fin attachment. The exception noted is that at $\lambda/L = 5.04$ and $\lambda/L = 1.50$, the mooring lines experienced lower force when the fin attachment was not removed. At 90° setup, the mooring force was lowest at $\lambda/L = 2.24$, representing a 25% reduction compared to the setup when the fin attachment was removed at the same λ/L. The fin attachment angle was set at 90°, and the variation in load was more gradual compared to when it was set at 0°, which helped prevent excessive instantaneous impacts on the mooring line.

As shown in Figure 9b, none of the different configurations exhibited a distinct load pattern as being the setup with the lowest mooring force. For the group with the fin attachment at different angles, the least mooring force occurred at $\lambda/L = 2.84$. It was observed that the setup with the 90° fin angle amongst others showed median force distribution.

4.3. Motions of the Model

Noting that the floating breakwater was moored in place by four mooring lines, the other motions not considered had been restricted by the force on the mooring lines, and since the model was confined to 2 dimensions, their motions were considered. In Figures 10–12, the pitch, heave, and surge expressed in terms of RAOs are illustrated for both the 3 cm and 5 cm incident waves amplitudes.

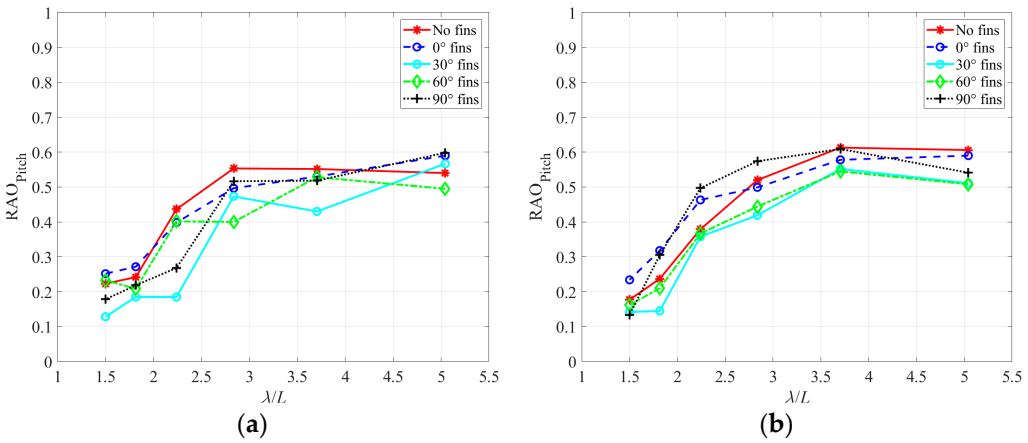

Figure 10. RAO of pitch (in radian) variation with λ/L for (**a**) 3 cm and (**b**) 5 cm incident wave amplitude.

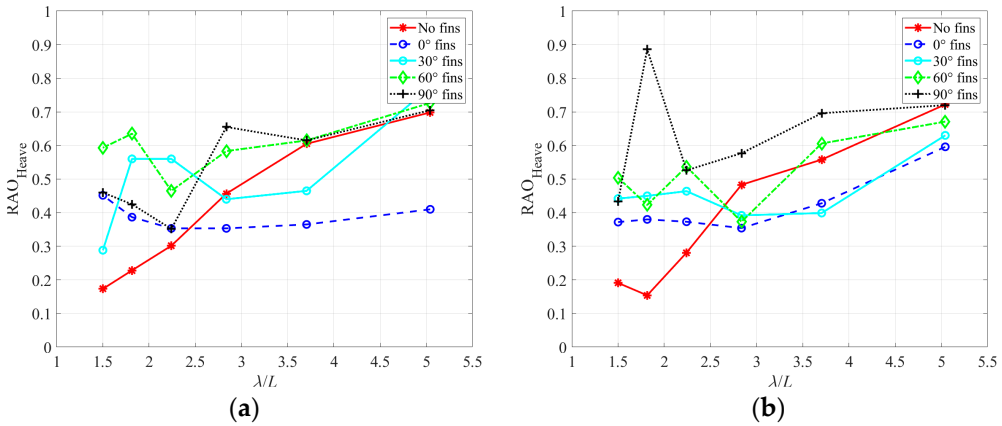

Figure 11. RAO of heave variation with λ/L for (**a**) 3 cm and (**b**) 5 cm incident wave amplitude.

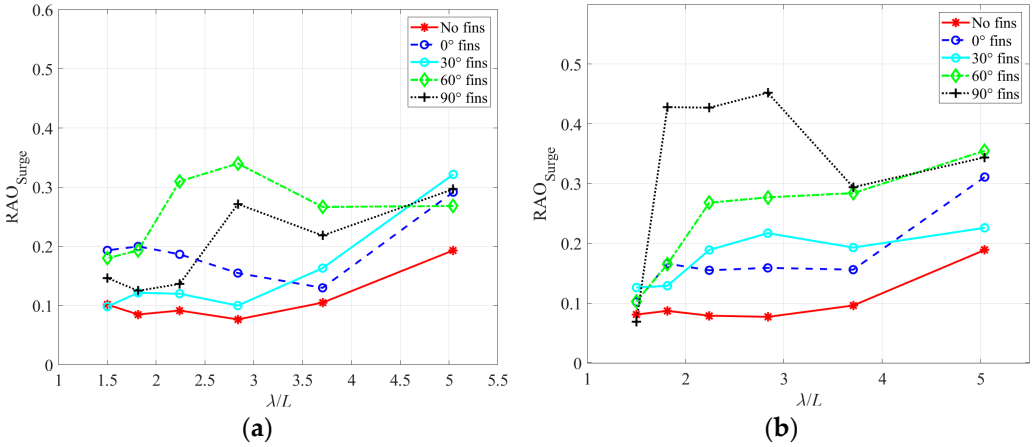

Figure 12. RAO of surge variation with λ/L for (**a**) 3 cm and (**b**) 5 cm incident wave amplitude.

One of the design objectives of any moored floating structure is accurate prediction of its motions to wave impacts, which is impulsive wave. This is as important to the service life of the structures as it is to its station-keeping and stability. The desire is to ensure minimum motions are experienced under the influence of wave loading. As illustrated in Figure 11a,b, the pitch RAO showed a decreasing trend as the incident λ/L increased for all the fin attachment angle types as well as the "no fin" setup. Since wave period is expressed as the inverse of λ/L, the pitch RAO was high in the long period wave regime ($\lambda/L > 3.71$). Also, for the pitch motion in the case of both the 3 cm and 5 cm incident wave amplitude, the configuration with fin attachment at 30° inclination showed the lowest pitch motion, reducing the pitch motion by up to 42% and 34%, respectively, relative to the setup with no fin attachment, which is the default setup.

Now, considering the heave RAO at both 3 cm and 5 cm incident wave amplitudes, the lowest motion was experienced by two different setup arrangements. Between the frequency range of $\lambda/L = 5.04$ and $\lambda/L = 2.24$, the setup with 0° fin inclination had the least heave motion, reducing the heave motion by 39% compared to the default setup, while beyond $\lambda/L = 2.24$ until $\lambda/L = 1.50$, the "no fin" setup showed the least heave motion. It implies that at 0°, the setup was most suitable in the low-frequency regime, whereas the "no fin" type performed better in the high-frequency region, as illustrated in Figure 12a,b.

In the context of surge motion response of the floating structure, the configuration with no fin attachment remarkably exhibited the least surge RAO. The fin attachment at all the angles considered had no significance in reducing surge motion in both instances of 3 cm and 5 cm incident wave amplitude.

5. Conclusions

A floating breakwater with bio-inspired fin attachments was developed and experimentally tested in this work. The fin attachment had a variable angle configuration. The angles can be changed from 0° steps of 30° to 90°. The experimental cases included four groups involving fin attachment and one group without. These five groups were tested in two main incident wave amplitudes of 3 cm and 5 cm. The five incident wave frequencies tested ranged from 0.6 Hz to 1.1 Hz. The combination of these variables totaled 60 experimental cases, to study the influence of fin attachment on wave attenuation, hydrodynamic motion of the structure, and tension force in the mooring lines.

The incident wave amplitudes selected in the experiment were suitable for the total height of the structure (24 cm) as smaller amplitudes would have an insignificant effect, while bigger ones would be beyond the FB's effective wave defence capacity. The data acquired from the experiment and data analyses revealed that for the wave impact attenuation, the 90° fin attachment was the best in attenuating waves of both 3 cm and 5 cm amplitudes. Compared with the control configuration, that with no fin attachment, the transmission coefficient, Kt, was reduced by as much as 74%. This implies that as up to

26% of the incident waves went past the breakwater to the downstream side, which is the protected area.

The hydrodynamic response analyses conducted in this report took into cognisance the pitch, heave, and surge motions, expressed in a dimensionless term referred to as RAOs for each of the motions. In terms of pitch RAO, 30° fin configuration exhibited the least motion. A reduction of up to 42% was realised compared to the control configuration. When pitch motion reduction is desirous, then, a fin inclined at 30° would effectively realise this goal. The fin has been reported to generate vortex at its edges, dissipating some parts of the incident waves energy. Considering the heave RAO, as much as 39% heave motion was reduced when the fin attachment was at 0° fin angle. In the horizontal position, the length of the breakwater effectively increased. Since the fins were installed on the upstream side and downstream of the FB, the length of the breakwater had increased by twice the effective length of the fins (1.5 cm) from 86 cm to 89 cm. Finally, the surge RAO was evaluated, and it was seen that none of the finned configurations effectively reduced the surge motion. The least surge motion occurred with the no-fin attachment setup.

It was noted that the finned configurations experienced the lowest mooring force at $\lambda/L = 0.33$ for both incident wave amplitudes. Moreover, the 90° fin attachment exhibited an average force distribution, comparatively. The best angle and configuration combination was the pontoon-type breakwater with 90° fins, as it provided the most effective wave attenuation, exerted smaller and more stable forces on the moorings, and ensured a longer service life.

Overall, this project's aims include defending marine structures from wave impact, reducing structural motions, and evaluating the tensile force imposed on the mooring system. The implication and applicability of these analyses are to protect marine structures from wave impact while enhancing the structural service life, such as floating solar systems [30].

Author Contributions: Conceptualization, X.L., C.M.T., L.A., M.F. and L.H.; methodology, Y.Y., C.M., S.C. and L.H.; formal analysis, X.L., C.M.T., L.A. and M.F.; investigation, Y.Y., C.M., B.O. and L.H.; resources, A.W., J.G.D. and L.H.; data curation, X.L., C.M., C.M.T., L.A., M.F. and S.C.; writing—original draft preparation, X.L., C.M.T., L.A. and M.F.; writing—review and editing, X.L., Y.Y., A.W., J.G.D. and L.H.; visualisation, X.L. and Y.Y.; supervision, Y.Y., C.M., B.O., S.C. and L.H.; project administration, L.H.; funding acquisition, L.H. All authors have read and agreed to the published version of the manuscript.

Funding: L.H. acknowledges grants received from Innovate UK (No. 10048187, 10079774, 10081314), the Royal Society (IEC\NSFC\223253, RG R2 232462), and UK Department for Transport (TRIG2023—No. 30066).

Data Availability Statement: All data underlying the results are available as part of the article and no additional source data are required.

Conflicts of Interest: Anson Wong and John Gordon Duffy were employed by DuPont. The remaining authors declare that the research was conducted in the absence of any commercial or financial relationships that could be construed as a potential conflict of interest.

References

1. Widagdo, A.B.; Sujoko, S.U.; Subarkah, A.; Aziiz, S.A.; Sukmana, C.I.; Saputra, A.D. Study of Wave Deformation Around Floating Breakwater. *J. Phys. Conf. Ser.* **2020**, *1625*, 012055. [CrossRef]
2. Koutandos, E.; Prinos, P.; Gironella, X. Floating breakwaters under regular and irregular wave forcing: Reflection and transmission characteristics. *J. Hydraul. Res.* **2005**, *43*, 174–188. [CrossRef]
3. Zhang, C.; Magee, A.R. Effectiveness of Floating Breakwater in Special Configurations for Protecting Nearshore Infrastructures. *J. Mar. Sci. Eng.* **2021**, *9*, 785. [CrossRef]
4. Cebada-Relea, A.; López, M.; Aenlle, M.L. Time-domain numerical modelling of the connector forces in a modular pontoon floating breakwater under regular and irregular oblique waves. *Ocean Eng.* **2022**, *243*, 110263. [CrossRef]
5. Sohrabi, S.; Lotfollahi Yaghin, M.A.; Mojtahedi, A.; Aminfar, M.H.; Dadashzadeh, M. Experimental and numerical investigation of a hybrid floating breakwater-WEC system. *Ocean Eng.* **2024**, *303*, 117613. [CrossRef]
6. He, F.; Li, J.; Pan, J.; Yuan, Z. An experimental study of a rectangular floating breakwater with vertical plates as wave-dissipating components. *Appl. Ocean Res.* **2023**, *133*, 103497. [CrossRef]

7. Mao, P.; Chen, C.; Chen, X.; Zhang, Q.; Bao, Y.; Yang, Q. An innovative design for floating breakwater with Multi-objective genetic optimal method. *Ocean Eng.* **2024**, *312*, 119202. [CrossRef]
8. Martinelli, L.; Ruol, P.; Zanuttigh, B. Wave basin experiments on floating breakwaters with different layouts. *Appl. Ocean Res.* **2008**, *30*, 199–207. [CrossRef]
9. Koo, W. Nonlinear time–domain analysis of motion-restrained pneumatic floating breakwater. *Ocean Eng.* **2009**, *36*, 723–731. [CrossRef]
10. Ji, C.; Bian, X.; Xu, S.; Guo, J.; Huo, F. Numerical study on the hydrodynamic performance of floating breakwaters with complex configurations. *Ocean Eng.* **2023**, *273*, 114032. [CrossRef]
11. Armono, H.; Suastika, K.; Ridlwan, A.; Biaperi, T. Numerical Study of Bilge Keel Length Variations of Floating Breakwater to Optimize Transmission Coefficient. In Proceedings of the 7th International Seminar on Ocean and Coastal Engineering, Environmental and Natural Disaster Management (ISOCEEN 2019), Singapore, 6–7 November 2019; pp. 191–197. [CrossRef]
12. Hajivalie, F.; Yeganeh-Bakhtiary, A.; Bricker, J.D. Numerical Study of the Effect of Submerged Vertical Breakwater Dimension on Wave Hydrodynamics and Vortex Generation. *Coast. Eng. J.* **2015**, *57*, 1550009-1–1550009-21. [CrossRef]
13. Jiang, Y.; Ding, Y.; Sun, Y.; Shao, Y.; Sun, L. Influence of bilge-keel configuration on ship roll damping and roll response in waves. *Ocean Eng.* **2020**, *216*, 107539. [CrossRef]
14. Dai, J.; Wang, C.M.; Utsunomiya, T.; Duan, W. Review of recent research and developments on floating breakwaters. *Ocean Eng.* **2018**, *158*, 132–151. [CrossRef]
15. Nasri, B.; Moghim, M.N.; Badri, M.A. Experimental study on trapezoidal pontoon-type floating breakwaters with attached porous plates. *J. Ocean Eng. Mar. Energy* **2021**, *7*, 41–57. [CrossRef]
16. Abul-Azm, A.G.; Gesraha, M.R. Approximation to the hydrodynamics of floating pontoons under oblique waves. *Ocean Eng.* **2000**, *27*, 365–384. [CrossRef]
17. Pena, B.; Muk-Pavic, E.; Thomas, G.; Fitzsimmons, P. Numerical analysis of a leading edge tubercle hydrofoil in turbulent regime. *J. Fluid Mech.* **2019**, *878*, 292–305. [CrossRef]
18. Chakrabarti, S.K. *Handbook of Offshore Engineering*; Elsevier Science & Technology: Amsterdam, The Netherlands, 2005; ISBN 978-0-08-044381-2.
19. MatWeb. DuPont Styrofoam Polystyrene Rigid Foam Insulation. 2021. Available online: https://www.matweb.com/search/DataSheet.aspx?MatGUID=c98422e64d1f4bfa98e9d82dc89eaee6 (accessed on 1 May 2024).
20. Vryhof Anchors B.V. *Vryhof Manual the Guide to Anchoring*, 5th ed.; Vryhof Anchors B.V.: Schiedam, The Netherlands, 2015; Volume 49, pp. 25–41.
21. DuPont™ Styrofoam™ Brand Highload 40, 60 and 100 Insulation. Available online: https://www.dupont.com/content/dam/dupont/amer/us/en/performance-building-solutions/public/documents/en/styrofoam-brand-highload-40-60-and-100-pis-43-D100079-enNA.pdf (accessed on 10 July 2024).
22. MatWeb. Aluminium 98% Al_2O_3. 2021. Available online: https://www.matweb.com/search/DataSheet.aspx?MatGUID=38cd8590a98f457a8f4bea462fe91cfa (accessed on 1 May 2024).
23. Lin, C.; Kao, M.-J.; Yang, J.; Raikar, R.V.; Yuan, J.-M.; Hsieh, S.-C. Similarity and Froude Number Similitude in Kinematic and Hydrodynamic Features of Solitary Waves over Horizontal Bed. *Processes* **2021**, *9*, 1420. [CrossRef]
24. Berends, E.E. Scaling Effects and Validation of the Ocean Grazer Experimental Wave Tank Using CFD. Master's Thesis, University of Groningen, Groningen, The Netherlands, 9 July 2021.
25. Edinburgh Designs. Flap Ocean Waves Generator. 2009. Available online: http://www4.edesign.co.uk/waves/ (accessed on 1 May 2024).
26. Ning, D.; Zhao, X.; Göteman, M.; Kang, H. Hydrodynamic performance of a pile-restrained WEC-type floating breakwater: An experimental study. *Renew. Energy* **2016**, *95*, 531–541. [CrossRef]
27. Huang, L.; Thomas, G. Simulation of wave interaction with a circular ice floe. *J. Offshore Mech. Arct. Eng.* **2019**, *141*, 041302. [CrossRef]
28. Brossard, J.; Jarno-Druaux, A.; Marin, F.; Tabet-Aoul, E.H. Fixed absorbing semi-immersed breakwater. *Coast. Eng.* **2003**, *49*, 25–41. [CrossRef]
29. Fatigue as a Phenomenon in the Material. In *Fatigue of Structures and Materials*; Schijve, J., Ed.; Springer: Dordrecht, The Netherlands, 2009. [CrossRef]
30. Yang, Y.; Mi, C.; Ou, B.; Wong, A.; Duffy, J.G.; Wood, T.; Utama, I.K.A.P.; Chen, W.; Huang, L. A comparative experimental study on the hydrodynamic performance of two floating solar structures with a breakwater in waves. *Sol. Energy* **2024**, *284*, 113029. [CrossRef]